Networked Control of Multiple Ultra-High-Speed PMSMs for AMEBA

Kazi Nishat Tasnim
Department of Electrical and Computer Engineering
Mississippi State University
Starkville, MS-39762, USA
kt1446@msstate.edu

Md. Khurshedul Islam
Department of Electrical and Computer Engineering
Mississippi State University
Starkville, MS-39762, USA
mi264@msstate.edu

Moinul Shahidul Haque
Controls Engineer
Nexteer Automive
Saginaw, Michigan 48601 US
moinul.haque@nexteer.com

Seungdeog Choi
Department of Electrical and Computer Engineering
Mississippi State University
Starkville, MS-39762, USA
seungdeog@ece.msstate.edu

***Abstract*— This paper presents a speed synchronization control of a networked multiple ultra-high-speed PMSMs (UHS-PMSM) of 0.5M rpm rated speed for a mechanically based antenna (AMEBA). Multiple UHS-PMSMs with the same speed can establish a much stronger and more reliable communication in radio-frequency (RF) denied environments such as underwater or underground facilities. Thus, speed synchronization within a finite time limit is inevitable for AMEBA applications. The proposed control scheme consists of two segments, a supervisory controller (SC) and an individual motor drive (IMD) system. The SC is proposed for minimizing the speed difference between each motor as well as from the reference speed, using a sliding mode controller (SMC). In the IMD system, an extended state observer (ESO), with a new switching function, is used for canceling further disturbances occurring from speed synchronization error and other external disturbances. A double-power-based sliding mode controller is used to regulate the current in the IMD system, and a deadbeat model predictive (DMP) controller is used for the voltage regulator. The proposed synchronous control system is validated through simulation and experiments under different operating conditions to establish its effectiveness for AMEBA application.**

Keywords—UHS-PMSM, Supervisory controller, Networked control, GaN-FET inverter.

I. Introduction

Ultra-high-speed permanent magnet synchronous machines (UHS-PMSM) are gaining popularity for their compact design, high power density, and high performance in medical applications, spindles, turbo compressors, and consistently growing high-speed applications [1][2]. AMEBA is one of the applications of UHS-PMSM for its high-fundamental frequency and high efficiency. AMEBA has been developed for communicating with submarines, unground mines, and underwater facilities. Such an RF-denied environment has a short skin depth of electromagnetic (EM) waves, which causes high attenuation of the transmission signal, thus hindering communication. However, it is observed that an electromagnetic field of 0.3kHz – 10kHz frequency can penetrate long distances but requires huge transmitters, which is not power-efficient [3]. A mechanical transmitter is proposed to replace enormous antennas for transmitting electric fields, where a magnetic dipole is oscillated by UHS-PMSM. However, the total moment of inertia of the magnet can increase

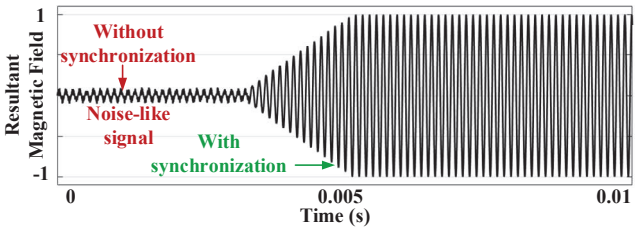

Fig.1. Overview of desired Magnetic Field

the power consumption of the motor drives rapidly when operated at high speed. So, the distributed transmitter is proposed, where a single magnet is divided into an array of magnets and driven by individual UHS-PMSM to minimize the moment of inertia. Synchronizing multiple UHS-PMSM speeds is crucial for getting the expected oscillating waveform; otherwise, the receiver would pick up noise-like signals [4], as shown in Fig. 1. A high-level diagram of the distributed AMEBA system is shown in Fig.2. Control of the whole networked UHS-PMSM system mainly imposes two challenges: the precise speed control of each UHS-PMSM and the synchronization among each motor.

Research on speed synchronization of multiple motors in the ultra-high-speed region is very limited. Moreover, for AMEBA, each motor must have high dynamic performance for correct message transmission. According to the AMEBA requirement, each motor should reach a steady state within 0.5s in the worst-case scenario, so synchronization should be achieved before that. Several synchronization processes have been studied before, such as master-slave, cross-coupling, adjacent coupling, and virtual spindle control [5]-[7]. In the master-slave controller, the slave takes command from the master, which induces a time delay in the system [5]. Moreover, the slave is considered undisturbed, which is not applicable for AMEBA as each motor is driven individually. Virtual spindle control is done offline, and any mismatch between offline sampling rate and real-time operation can cause instability [6]. Cross-coupling and adjacent coupling between consecutive motors have been shown to address these issues in [7] and [8]. [7] presents an intelligent supervisory control system based on the cross-coupling method; however, a master motor works as a centralized controller that limits the dynamic performance of each motor, as it induces time delay. For solving centralized

2022 IEEE Energy Conversion Congress and Exposition (ECCE) | 978-1-7281-9387-8/22/$31.00 ©2022 IEEE | DOI: 10.1109/ECCE50734.2022.9947642

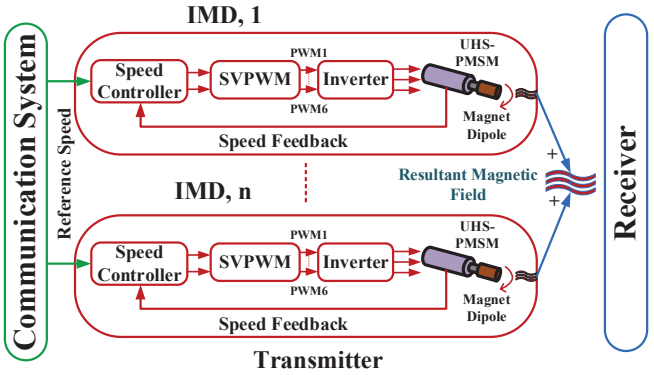

Fig. 2. High-level distributed AMEBA system

control, [8] presents a cross-coupling method combined with SMC. However, individual motor steady-state performance shows chattering, which is not acceptable for AMEBA, as chattering is considered as noise to the receiver.

High dynamic performance of each motor is as crucial as speed synchronization control for AMEBA. However, the performance of the UHS-PMSM drive is severely affected by some issues, such as motor parameter variation and increasing non-linearity of the system model due to the high fundamental frequency of 8.33kHz. Existing PI and Fuzzy logic controllers can deal with the increasing non-linearity by adopting self-tuned gain values. However, these methods cannot adapt to disturbances such as motor structure parameter variation and load torque change [9]. A non-linear controller such as a sliding mode controller (SMC) is used for robustness and disturbance rejection capability [10]-[12]. [10] presents non-singular terminal sliding mode surface-based control; however, chattering is a prominent issue of this controller. To address this, [11] and [12] present reaching law-based SMC to reduce chattering. However, the error gain value has to be larger than the upper bound of lumped disturbance; otherwise, chattering remains.

So, to address the abovementioned issues, a new switching function-based ESO system is proposed here to estimate the IMD drive system disturbance, and disturbance compensated speed feedback is estimated. Estimated feedback speed is given input to the supervisory controller. A circular error model is designed in the SC system to converge the error among neighboring motors to zero. In SC, a simple reaching law-based SMC system is used to reduce complexity. Then the minimized synchronous error is given input to the IMD system's double-power reaching law-based SMC current regulator, which is able to reduce chattering and reach steady-state within a finite time. A testbed with three UHS-PMSMs is developed for validating the proposed network control system.

The rest of the paper is organized as follows. Section II discussed about the performance requirement of UHS-PMSM for AMEBA. Section III broadly discusses the theory and mathematics of the control system, section IV presents validation through simulation, section V presents experimental validation, and finally concludes with section VI.

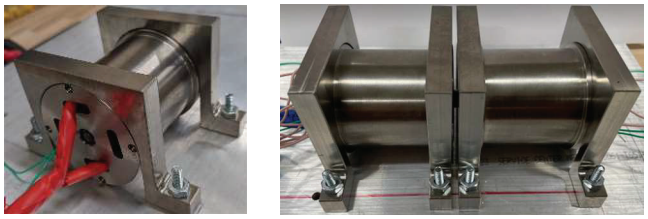

Fig.3. (a) UHS-PMSM and (b) dynamometer.

Table I
UHS-PMSM MODEL PARAMETER

Parameter	Symbol	Value
Stator Resistance	R	0.1382Ω
Stator Inductance	$L_d = L_q$	$65\times 10^{-6}H$
Flux Linkage	λ_{pm}	$.0032Wb$
Inertial Coefficient	J	3.8×10^{-6}
Friction Coefficient	B	2×10^{-7}
Rated Power	P_{rated}	2kW
Rated Current	I_{rated}	6.3A rms
Pole Pair	P	1
Rated Speed	ω_{rated}	500k r/min
Rated Torque	T_{rated}	40mNm

II. Performance Requirement of UHS-PMSM

A prototype of UHS-PMSM is developed with 2kW rated power and 0.5M rpm rated speed. It has a slot-less stator and surface-mounted rotor. Fig. 3. shows the prototype and a dynamometer developed with two UHS-PMSMs.

As, the UHS-PMSM behaves like a surface-mounted motor, d-axis and q-axis stator inductance have the same value, $L_d = L_q = L_s$. The mathematical model of the UHS-PMSM is presented in (1).

$$\left.\begin{aligned} v_d &= L_s\frac{di_d}{dt} + R_s i_d - L_s P\omega i_q \\ v_q &= L_s\frac{di_q}{dt} + R_s i_q + L_s P\omega i_d + P\omega\lambda_{pm} \\ \dot{\omega} &= \frac{\{(1.5P\lambda_{pm}i_q - T_l) - B\omega\}}{J} \\ T_e &= 1.5P\lambda_{pm}i_q \end{aligned}\right\} \quad (1)$$

Here, ω is the mechanical speed, T_e is the electrical torque, L_s is the stator inductance, J is the rotor inertia, B is the friction coefficient, λ_{pm} is the permanent magnet flux linkage, P is the number of pole pairs and, v_{dq} and i_{dq} is the voltage and current in a stationary frame. Table I, shows the parameter values of the motor.

In AMEBA, a digital communication system is translated into analog frequencies, as shown in Fig. 4. These frequencies are the speed command of each motor. So, correct communication depends on the dynamic speed performance of the UHS-PMSM. For being accurately received by the receiver in the RF-denied environment, speed has to settle down before 0.5s, and overshoot should be less than 1.2%. For distributed AMEBA system, all the motors must reach synchronization

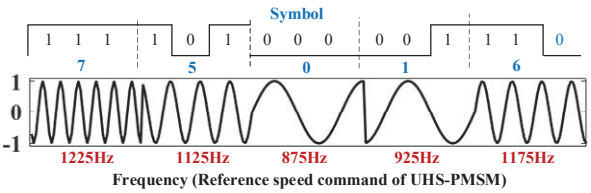

Fig. 4. Interpretation of reference speed from digital communication signal

quickly to prevent the receiver from interpreting the noisy signal.

III. Proposed Theory

Synchronism among the motors can be disturbed by various factors, such as different gain coefficients in different IMDs and a different load torque of different UHS-PMSMs. All the UHS-PMSMs are operated with the same reference speed. However, parameter variation, such as stator resistance and permanent magnet flux linkage, can disturb individual motor drive performance. So here, an ESO-based supervisory controller is proposed to ensure both speed synchronization of multiple UHS-PMSM and individual motor dynamic performance. A detailed mathematical model of the proposed model is described in this model. Here, (·) on a variable indicates derivative, and (^) on a variable indicates the estimated value of the variable.

A. An extended State Observer System

This segment deals with the disturbance estimation of each individual UHS-PMSM. At the Ultra-high-speed region, the coil and magnet temperature of PMSM rises, which introduces some structure parameter variation, such as stator resistance and flux linkage variation. Stator resistance tends to increase with increasing coil temperature, and Flux linkage reduces with increasing magnet temperature. These variations can cause chattering in a steady state speed response. Load torque variation is also considered a disturbance in this paper, so that UHS-PMSM can keep the commanded speed in sync with the neighboring motors. After estimating disturbance compensated speed, $\widetilde{\omega}_k$, its given input to the supervisory control, described in the next section. And the estimated disturbance is given input to the sliding mode-based current controller.

UHS-PMSM speed can be defined as equation (2) from (1).

$$\dot{\omega} = Ai_q - E\omega - FT_l \tag{2}$$

Here, $A = (1.5P\lambda_{pm})/J$, $E = B/J$, and $F = 1/J$. Now, for modeling disturbances, perturbation is added with the sensitive parameters, such as A, i_q and T_l. So, (2) can be rewritten as (3)

$$\begin{aligned} \dot{\omega} &= (A + \Delta A)(i_q + \Delta i_q) - E\omega - FT_l \\ \dot{\omega} &= Ai_q(t) - E\omega(t) - D(t) \\ D(t) &= \Delta\dot{\omega} + FT_l - \Delta X\Delta i_q - X\Delta i_q \\ &\quad - \Delta X i_q \end{aligned} \tag{3}$$

Now, comparing the first equation of (3) with the first-order single input single output (SISO) system, i_q can be defined as the control input, and $D(t)$ can be defined as the uncertainties.

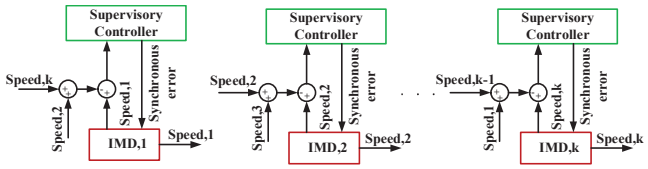

Fig. 5. Synchronization error model

For Designing the ESO system, an extended state $d(t)$ is added, and the states are written as (4).

$$\begin{aligned} \dot{\hat{\omega}}(t) &= -E\hat{\omega}(t) + Ai_q - d(\varepsilon(t)) \\ \dot{d}(\varepsilon(t)) &= d(t) - \xi_2\varepsilon(t) \\ \dot{d}(t) &= -\xi_1 h(\varepsilon(t)) \end{aligned} \tag{4}$$

Here, ξ_1 *and* ξ_2 are disturbance coefficients, $h(t)$ is the switching function that tracks the change of disturbance, and it is defined as (5).

$$h(\varepsilon) = \left(2\,arctan(\exp(4\varepsilon)) - \frac{\pi}{2}\right) \tag{5}$$

In (4), $\hat{\omega}$ is tracking the feedback speed ω, whereas $d(t)$ is tracking the uncertainties. When the system converges, speed error, $\varepsilon(t) = \hat{\omega}(t) - \omega(t)$ converges to zero and estimated disturbance, $d(t)$ reaches a constant value. So, estimated disturbance compensated speed can be written as (6).

$$\dot{\hat{\omega}}(t) = -E\hat{\omega}(t) + Ai_q(t) + d(t) - \xi_2\varepsilon(t) \tag{6}$$

After this module, estimated speed, $\hat{\omega}$ goes to the supervisory controller for minimizing the synchronous error among multiple motors, and disturbance $d(t)$ goes to the current regulator for obtaining optimal current value.

B. Supervisory Controller (SC)

Errors among the multiple-motors are designed in a circular coupling manner to be converged to zero, as shown in Fig. 5. So, the speed of each motor is compared with the neighboring ones to be synchronized.

Individual motor speed errors with respect to the reference speed is expressed as (7).

$$\begin{aligned} err_1 &= \omega_{ref} - \widetilde{\omega}_1 \\ err_2 &= \omega_{ref} - \widetilde{\omega}_2 \\ &\vdots \\ err_k &= \omega_{ref} - \widetilde{\omega}_k \end{aligned} \tag{7}$$

Here, ω_{ref} is the reference speed and $\widetilde{\omega}_k$ is the estimated motor speed of k^{th} UHS-PMSM. Now, the speed error of each motor is compared with the neighboring motor speed error to define the synchronous speed error as (8).

$$\begin{aligned} E_1 &= err_1 - err_2 \\ E_2 &= err_2 - err_3 \\ &\vdots \\ E_k &= err_k - err_1 \end{aligned} \tag{8}$$

Now, the synchronous error of each motor can be defined as (9).

$$e_{syn,k} = E_k - E_{k-1}$$
$$e_{syn,k} = 2\tilde{\omega}_k - \tilde{\omega}_{k-1} - \tilde{\omega}_{k+1} \quad (9)$$

For designing the supervisory controller, the exponent reaching law is used for converging the error to zero. Exponent reaching law and integral sliding surface for each motor is presented as (10) and (11).

$$\frac{ds_k}{dt} = -k_{1,syn}s_k - k_{2,syn}sgn(s_k) \qquad k_1, k_2 > 0 \quad (10)$$

$$s_k = e_{syn,k} + C_{syn}\int_0^t e_{syn,k}(\tau)d\tau \quad (11)$$

Now, by differentiating (11), we get (12).

$$\dot{s}_k = \dot{e}_{syn,k} + C_{syn}e_{syn,k} \quad (12)$$

After differentiating, equating (12) with (10) gives us,

$$-k_{1,syn}s_k - k_{2,syn}sgn(s_k) = \dot{e}_{syn,k} + C_{syn}e_{syn,k}$$

Now, from (7), (8), and (9), the synchronous error of each motor can be defined as equation (13).

$$e_{syn,k} = \{C_{syn}e_{syn,k-1} + C_{syn}e_{syn,k+1} - (2\tilde{\omega}_k - \tilde{\omega}_{k-1} - \tilde{\omega}_{k+1}) - k_{1,syn}s_k - k_{2,syn}sgn(s_k)\}/2C_{syn} \quad (13)$$

C. Reaching Law-Based Current Regulator

In this segment, the optimal current value is obtained by converging synchronous error and individual motor speed error with respect to the reference value to zero. The total error is designed as (14).

$$e_{tot,k} = e_{syn,k} + e_k \quad (14)$$

Here, e_k is individual motor error defined as, $e_k = \omega_{ref} - \hat{\omega}$ and ω_{ref} is the reference speed for all the motors.

Now, reaching a law-based sliding mode controller is used to eliminate total error. Reaching law is gaining popularity as it directs the system states to the sliding surface within a finite time. Traditionally, exponent reaching laws are used in sliding mode control as described in (10). However, for the AMEBA application, the speed response of each UHS-PMSM has to be chattering-free and quick. So, for the IMD system, double power-based reaching law is proposed, and it is defined as (15)

$$\frac{ds}{dt} = -k_1|s|^{h_1}s - k_2|s|^{h_2}sgn(s);\ k_1, k_2 > 0$$
$$h_1 = \tanh(s^{\gamma_1}) - \left(2\,arctan(\exp(4\gamma_2 s)) - \frac{\pi}{2}\right) \quad (15)$$
$$h_2 = \gamma_3\left(2\,arctan(\exp(4\gamma_2 s)) - \frac{\pi}{2}\right)$$

Where, $\gamma_1, \gamma_2, and\ \gamma_3$ are positive definite constants. The fluctuation of system states causes chattering once they reach the sliding surface. With exponent reaching law, system states tend to fluctuate even after reaching zero error states. So,

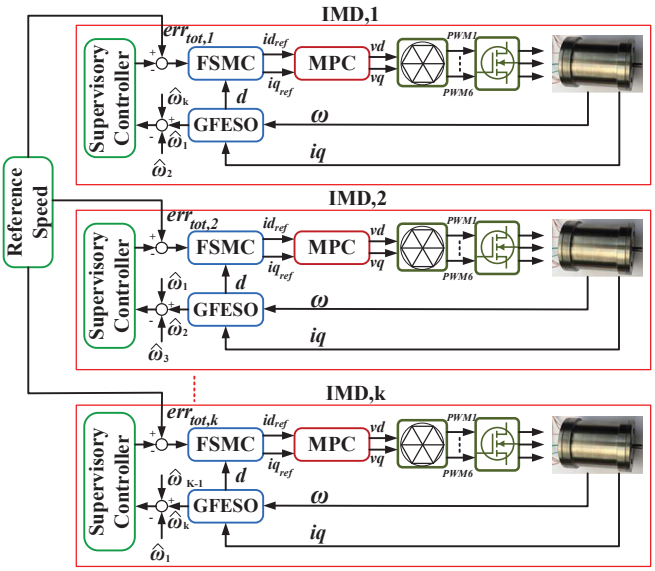

Fig. 6. Detailed block diagram of the proposed control system

steady-state chattering originates. Double power-based reaching law can address this issue as the fluctuation converges to zero as the system states converge to zero error. The Fluctuation band is defined as (16).

$$\Delta_2 = 2\frac{k_2 T|s(n)|^{h_2(n)}}{1 - k_1 T|s(n)|^{h_1(n)}} \quad (16)$$

The value of Δ_2 gradually converges to zero as the value of s reaches zero. Now, integral sliding surface is chosen as, (17).

$$s = e_{tot,k} + C\int_0^t e_{tot,k}(\tau)d\tau \quad (17)$$

Now, differentiating (17) and comparing it with (15) gives us

$-k_1|s|^{h_1}s - k_2|s|^{h_2}sgn(s) = \dot{e_{tot,k}} + C(e_{tot,k})$. Now from equations (7), (8), (9), and (2), the optimal current value can be determined as (18).

$$i_{qref} = (\dot{\omega}_{ref} + E\hat{\omega} - d + \xi_2\varepsilon + k_1|s|^{h_1}s + k_2|s|^{h_2}sgn(s) + C(err_k) + \dot{e_{tot,k}})/A \quad (18)$$

D. Deadbeat Model Predictive (DMP)based Voltage Regulator

For each IMD system, PI is replaced by DMP to avoid the inner current loop, as inner PI loop has limited frequency bandwidth, which limits the dynamic performance of the USH-PMSM. DMP uses the mathematical model of USH-PMSM to define stationary frame voltage. So, by discretizing the first two equations of (1), v_d and v_q can be written as (19).

$$v_q(n) = R\left(1 - e^{-\frac{R}{L}T_s}\right)^{-1}\left(i_q(n+1) - i_q(n)e^{-\frac{R}{L}T_s}\right) + E_q$$
$$v_d(n) = R\left(1 - e^{-\frac{R}{L}T_s}\right)^{-1}\left(i_d(n+1) - i_d(n)e^{-\frac{R}{L}T_s}\right) + E_d \quad (19)$$

Table II
Parameters of ADSM

Parameter	Symbol	Value
Disturbance coefficient in ESO	ξ_1	0.01
Error coefficient in ESO	ξ_2	1500
Reaching law coefficients in IMD	k_1	5
	k_2	13
First power term coefficients in IMD	γ_1	100
	γ_2	100
Second power term coefficient in IMD	γ_3	0.5
Error coefficient in IMD	C	35
Reaching law coefficients in SC	$k_{1,syn}$	0.01
	$k_{1,syn}$	0.01
Error Coefficient in IMD	C_{syn}	100

Here, E_{dq} presents the back EMF of UHS-PMSM, T_s is the sampling time and n is the sampling number.

The detailed control block of the proposed speed synchronization control system is shown in Fig. 6.

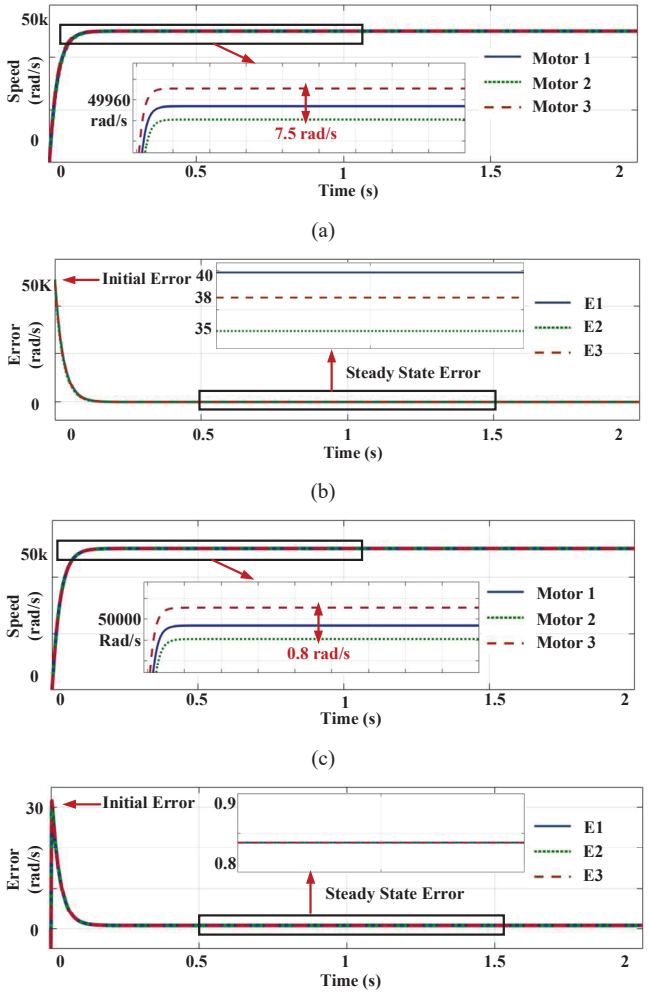

Fig. 7. Under different gain values, the speed response of three motors (a) without synchronization and (c) with synchronization. The error between motor (b) without synchronization and (d) with synchronization.

Table III
Gain coefficients

	IMD,1	IMD,2	IMD,3
Reaching law coefficient in IMD, k_1	5	10	15
Reaching law coefficient in IMD, k_2	13	23	33
Error coefficient in IMD, C	35	30	40

E. Stability Analysis

Lyapunov stability is used to maintain the stability of the IMD system. The energy of the system is used as the Lyapunov function.

$$V(x) = \frac{1}{2}s^2$$

For being asymptotically stable,

$$\dot{V}(x) = s\dot{s} < 0$$

By solving this inequality, it can be said that disturbance coefficients must be defined as positive definite values, as ξ_1>1 and ξ_2>1.

IV. Simulation Results

The proposed multiple motor networked control is validated by observing the motors' dynamic motor performance synchronization property. Error among each motor is observed with and without supervisory controller and the effectiveness of the proposed control scheme is validated under different operating conditions. For simulation optimization purposes, three UHS-PMSMs are used for validation, so $k = 3$ in all cases. Under normal conditions, gain coefficients are parameterized in table II.

A. With Different Reaching Law and Error Coefficient

The reaching law coefficients are k_1 and k_2, as described in equation (15). These coefficients contribute to the steady-state performance, and error coefficient C contributes to the transient performance of the motor. So, if different motors have different coefficients, their steady-state performance will lose synchronization. For analyzing the speed synchronization of each IMD system under different coefficient values, each motor is operated with the rated speed, ω_{ref}=50000 rad/s and no-load condition. The coefficient values of each motor are given in Table III.

From Fig. 7a and 7b, its seen that, without a supervisory controller for speed synchronization, each motor has a 37.5 rad/s speed difference from the reference speed on average and speed error from each other is 7.5 rad/s on average. Whereas with the SC system, each motor has almost 0 rad/s speed difference from reference speed, and speed error from each other is 0.8 rad/s on average, which is very negligible.

B. Load Torque Change

For validating the control scheme under different load torque changes, the load is changed to 1.5e-3 Nm, 2.5e-3 Nm,

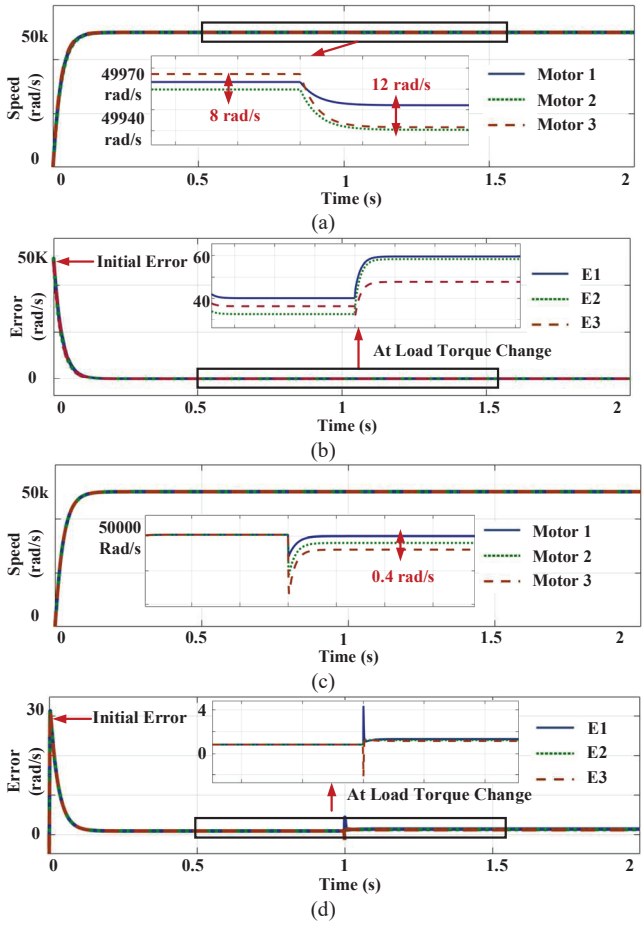

Fig. 8. Under different load torque changes, the speed response of three motors (a) without synchronization and (c) with synchronization. The error between motor (b) without synchronization and (d) with synchronization.

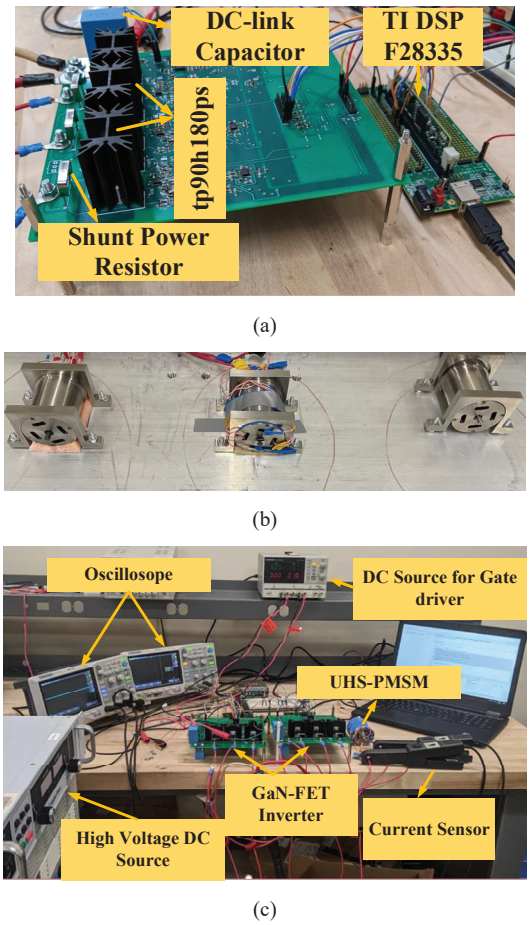

Fig. 9: Experimental Setup, (a) three-phase GaN-FET inverter, (b) Multiple UHS-PMSM setup and (c) testbed.

and 3.5e-3 Nm in IMD,1, IMD,2, and IMD,3 respectively at 1s. Reference speed for all the motors is, ω_{ref}=50000 rad/s. Fig. 8 shows the speed response of each motor under load torque change. Figures 8a and 8b show that, before load torque change, the difference between each motor is 8 rad/s and the average difference from reference speed is 40 rad/s. However, after load torque change at 1s, the error between motor increases to 12 rad/s, and the discrepancy from reference speed increases to 60 rad/s. This means that without speed synchronization and ESO system, the IMD system cannot regain the reference speed after load torque change and speed synchronization increases. Moreover, without SC, IMDs have an initial error of 50k rad/s, which is reduced to 30 rad/s with an SC system in both cases. So, it can be said that both steady-state and transient errors have been improved with the SC system.

V. Experimental Validation

A cascode GaN-FET-based three-phase inverter has been developed with phase current and DC voltage sensors. Three UHS-PMSM prototypes have also been developed to validate the proposed speed synchronization control. Fig. 9 shows the inverter and the testbench used here. Each UHS-PMSM has the same drive system, and three TI-DSP F28335s are used for interfacing. Real-time current and speed data are collected and processed in the mathematical model of the setup in MATLAB.

A. With Different Reaching Law and Error Coefficients

For experimental validation of the speed synchronization under the different gain and coefficient values as described in segment A of the previous section, the motor is operated at ω_{ref} =10k rad/s reference speed and no-load condition. Disturbance and error coefficients are changed as previously described in Table III. From Fig. 10a and 10b, its seen that, without a supervisory controller for speed synchronization, each motor has a 370 rad/s speed difference from the reference speed on average and speed error from each other is 36 rad/s on average.

Whereas with the SC system, each motor has almost 0 rad/s speed difference from reference speed, and speed error from each other is very negligible.

B. Load Torque Change

Each motor is driven with different load torque for observing the speed response of each IMD under loaded conditions. Load torque is changed at 1s to 0.007Nm, 0.008Nm and to 0.009Nm in IMD,1, IMD,2 and IMD,3 respectively. Reference speed for all of them is ω_{ref}=10000 rad/s. In this

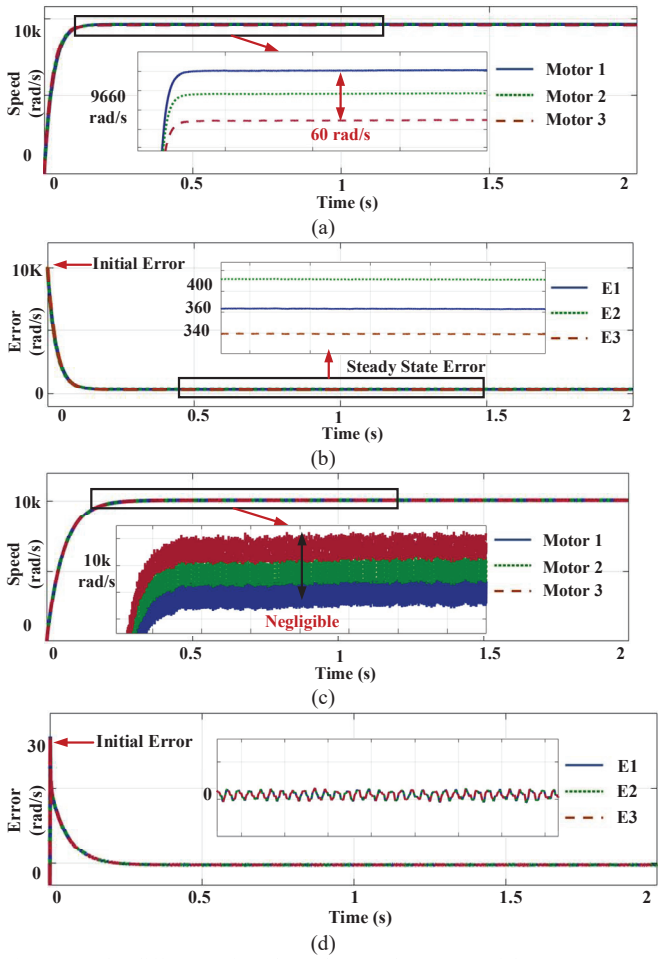

Fig. 10. Under different gain values, the speed response of three motors (a) without synchronization and (c) with synchronization. The error between motor (b) without synchronization and (d) with synchronization.

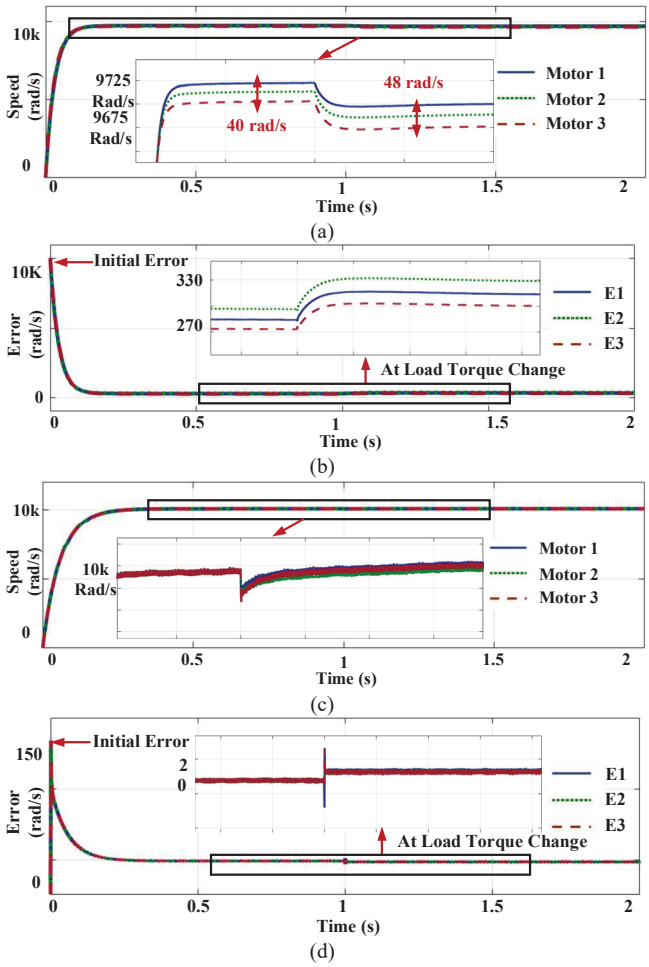

Fig. 11. Under different load torque change, speed response of three motors (a) without synchronization and (c) with synchronization. Error between each motor (b) without synchronization and (d) with synchronization.

case, all the gain and coefficient values of all the IMDs are kept the same as describedin Table II. Fig. 11 shows the speed response of three IMDs, with and without the SC system.

From Fig. 11a and 11b, its observed that, after load torque change at 1s, speed drops from 9725 rad/s to 9675 rad/s, and error between each IMD increases from 40 rad/s to 48 rad/s on average. Whereas, from Fig. 11c and 11d, speed is regained very quickly after load torque change. Moreover, the average speed error of each IMD from the reference speed is almost zero. The difference between each IMD speed response increases from 0 rad/s to 2 rad/s on average. In both cases, the initial error reduces from 10k rad/s to 30 rad/s by combining the SC system with ESO. So, the experimental results match the pattern of the simulation results.

VI. Conclusion

This paper proposes a speed synchronization method of a networked system of multiple UHS-PMSMs for a distributed AMEBA system. Speed synchronization of each motor is crucial for sending out the correct message in an RF-denied environment. Here, a supervisory controller (SC) is presented, and the error between each UHS-PMSM is modeled based on a circular coupling manner. A new switching function-based ESO system is combined with SC to further eliminate external disturbances and synchronous error. The proposed control system is validated through simulations and experiments. The error between each motor is reduced from 45 rad/s to almost zero and error from reference speed to 350 rad to a negligible value with the synchronized control system.

Acknowledgement

This research is supported by the National Science Foundation (NSF) CCSS-Comms Circuits and Sens System Program (Award# 1905434).

References

[1] C. J. V. Filho, D. Xiao, R. P. Vieira and A. Emadi, "Observers for High-Speed Sensorless PMSM Drives: Design Methods, Tuning Challenges and Future Trends," in IEEE Access, vol. 9, pp. 56397-56415, 2021, doi: 10.1109/ACCESS.2021.3072360.

[2] J. Luomi, C. Zwyssig, A. Looser and J. W. Kolar, "Efficiency Optimization of a 100-W 500 000-r/min Permanent-Magnet Machine Including Air-Friction

Losses," in IEEE Trans. on Ind. App., vol. 45, no. 4, pp. 1368-1377, July-aug. 2009.
[3] J. S. Glickstein, J. Liang, S. Choi, A. Madanayake and S. Mandal, "Power-Efficient ELF Wireless Communications Using Electro-Mechanical Transmitters," in *IEEE Access*, vol. 8, pp. 2455-2471, 2020.
[4] M. T. B. Tarek et al., "Power-Efficient Data Modulation for All-Mechanical ULF/VLF Transmitters," 2018 IEEE 61st International Midwest Symposium on Circuits and Systems (MWSCAS), 2018, pp. 759-762, doi: 10.1109/MWSCAS.2018.8623824.
[5] L. Qiu, Y. Shi, B. Zhang, J. Pan and X. Lai, "Tracking Control of Networked Multiple Linear Switched Reluctance Machines Control System Based on Position Compensation Approach," in IEEE Transactions on Industrial Informatics, vol. 14, no. 12, pp. 5368-5377, Dec. 2018, doi: 10.1109/TII.2018.2810538.
[6] Y. Wang, W. Zhang and L. Yu, "GESO-Based Position Synchronization Control of Networked Multiaxis Motion System," in IEEE Transactions on Industrial Informatics, vol. 16, no. 1, pp. 248-257, Jan. 2020, doi: 10.1109/TII.2019.2915321.
[7] F. -J. Lin, P. -H. Chou, C. -S. Chen and Y. -S. Lin, "DSP-Based Cross-Coupled Synchronous Control for Dual Linear Motors via Intelligent Complementary Sliding Mode Control," in IEEE Transactions on Industrial Electronics, vol. 59, no. 2, pp. 1061-1073, Feb. 2012, doi: 10.1109/TIE.2011.2157286.
[8] Q. Chen, F. Dong, L. Tao and Y. Nan, "Multiple motors synchronization based on active disturbance rejection control with improved adjacent coupling," 2016 35th Chinese Control Conference (CCC), 2016, pp. 4510-4516, doi: 10.1109/ChiCC.2016.7554054.
[9] R. Errouissi, A. Al-Durra and S. M. Muyeen, "Experimental Validation of a Novel PI Speed Controller for AC Motor Drives With Improved Transient Performances," in IEEE Transactions on Control Systems Technology, vol. 26, no. 4, pp. 1414-1421, July 2018, doi: 10.1109/TCST.2017.2707404.
[10] S. Li, M. Zhou and X. Yu, "Design and Implementation of Terminal Sliding Mode Control Method for PMSM Speed Regulation System," in IEEE Transactions on Industrial Informatics, vol. 9, no. 4, pp. 1879-1891, Nov. 2013, doi: 10.1109/TII.2012.2226896.
[11] Y. Zhang, Z. Yin, Y. Zhang, J. Liu and X. Tong, "A Novel Sliding Mode Observer With Optimized Constant Rate Reaching Law for Sensorless Control of Induction Motor," in IEEE Transactions on Industrial Electronics, vol. 67, no. 7, pp. 5867-5878, July 2020, doi: 10.1109/TIE.2019.2942577.
[12] X. Zhang, L. Sun, K. Zhao and L. Sun, "Nonlinear Speed Control for PMSM System Using Sliding-Mode Control and Disturbance Compensation Techniques," in IEEE Transactions on Power Electronics, vol. 28, no. 3, pp. 1358-1365, March 2013, doi: 10.1109/TPEL.2012.2206610.